DETECTION OF DEFECTS OF *CERASUS HUMILIS* FRUITS BASED ON HYPERSPECTRAL IMAGING AND CONVOLUTIONAL NEURAL NETWORKS
/
基于高光谱成像和卷积神经网络的欧李果实缺陷检测

Bin WANG [1], Lili LI [*1]
[1] College of Information Science and Engineering, Shanxi Agricultural University, Taigu 030800 / China
Tel: 18306832356; E-mail: lilycqdxyjs@163.com
DOI: https://doi.org/10.35633/inmateh-71-08

Keywords: *cerasus humilis fruits, natural defects, convolutional neural networks, hyperspectral imaging technology*

ABSTRACT
In order to perform highly effective identification of external defects and increase the additional value of Cerasus Humilis fruits, this study used hyperspectral imaging technology to collect information on intact and defective Cerasus Humilis fruits. Based on the full transition spectrum, partial least squares discriminant analysis (PLS-DA) and back propagation neural networks (BPNN) were used to establish a discriminative model. The competitive adaptive reweighted sampling (CARS) was used to extract feature wavelengths, principal component analysis was used for data compression of single band images, BPNN and convolutional neural networks (CNN) were used for defect Cerasus Humilis fruits recognition of principal component images. The results showed that the overall detection accuracy of PLS-DA and BPNN models based on wavelength spectral information were 83.81% and 85.71%, respectively. BPNN was used to establish the calibration model based on the selected characteristic wavelengths by CARS, the accuracy rate was 90.47%. The classified accuracy of CNN model based on principal component images was 93.33%, which was obviously better than that of BPNN model at 83.81%. The research shows that the CNN model was successfully applied to the detection of Cerasus Humilis fruits defects using hyperspectral imaging. This study provides a theoretical basis for the development of fruit grading and sorting equipment.

摘要
为实现欧李果缺陷特征的识别，提高欧李果附加价值，采用高光谱成像技术采集了完好和缺陷欧李果的信息。基于全渡段光谱，采用偏最小二乘判别分析 (Partial Least Squares-Discriminant Analysis, PLS-DA) 和误差反向传播神经网络 (Back Propagation Neural Networks, BPNN) 建立判别模型。采用竞争自适应加权(CARS)提取特征波长，并利用主成分分析进行单波段图像的数据压缩，针对主成分图像采用BPNN和卷积神经网络(Convolutional Neural Networks, CNN) 进行缺陷欧李果识别。结果表明，基于全波段光谱建立的PLS-DA、BPNN模型的整体判别正确率分别为83.81％和85.71%；采用CARS提取样本的特征波长后所建BPNN判别模型的正确率为90.47%；基于主成分图像建立的BPNN和CNN模型的判别正确率分别为83.81%和93.33%。研究表明，CNN可成功应用于基于高光谱技术的鲜枣黑斑特征识别中，该研究为开发水果的分级分选设备提供了理论基础。

INTRODUCTION

Cerasus Humilis fruits not only have a unique flavor, but is also rich in sugars, amino acids, proteins, vitamins, flavonoids, and other components. However, external defects such as rust spots, insect pests, and cracks on the surface of *Cerasus Humilis* fruits not only reduce the quality and price of the fruit but also easily cause fungi to infect other intact fruits, causing serious economic losses *(Wang et al., 2023)*.

Defect detection is an important aspect of fruit safety testing. At present, the detection of *Cerasus Humilis* fruits mainly relies on manual sorting, which involves manually sorting out irregular and damaged fruits, and then using existing grading equipment for size grading before being packaged and sold. Due to the low efficiency and accuracy of manual sorting, it is also difficult to sort *Cerasus Humilis* fruits with natural defects. Hyperspectral imaging technology has the advantages of being fast, non-destructive, and real-time, and has been successfully applied in the detection of fruit diseases such as pears *(Zhang et al., 2022)*, apples *(Gao et al., 2022)*, *Cerasus humilis* fruits *(Wang et al., 2023)*, and winter jujubes *(Jiang et al., 2023)*. In the external quality inspection of fruits, relevant research has been mainly focused on insect pests *(Liu et al., 2016)*, cracks *(Yu et al., 2014)*, and black spots *(Ye et al., 2022)* to achieve the classification of various defects and intact samples.

In modeling methods, convolutional neural networks, as a typical deep learning technique, can extract more abstract features and have been well applied in image processing and other fields *(Khaw et al., 2017; Fazari et al., 2021; Gai et al., 2022)*. In hyperspectral imaging, there are many spectral channels with high spatial variability. *Chen et al. (2018)* used convolutional neural networks (CNN) for hyperspectral classification, providing a feasible basis for fruit CNN hyperspectral detection. *Xue et al. (2020)* proposed using the GoogLeNet deep transfer model to detect apple defects and compared it with traditional machine learning methods. The results showed that the GoogLeNet deep transfer model has better generalization ability and robustness. *Zhu et al. (2019)* used near-infrared hyperspectral imaging technology to obtain spectral data for three soybean varieties and established a 1D-CNN model to distinguish soybean varieties. Research has shown that the classification accuracy of this model for each variety is above 90%. *Singh et al. (2021)* used a hyperspectral imaging system (900-1700 nm) to collect hyperspectral reflectance images of the ventral and dorsal sides of barley seeds, and the constructed CNN model had an accuracy of more than 98% in the test set.

This study aims to explore the feasibility of Hyperspectral imaging (HSI) combined with CNN for the identification of *Cerasus Humilis* fruit defects. The objectives of this study are as follows: (1) Collect hyperspectral images of intact and defective *Cerasus Humilis* fruit samples, extract average spectral data of regions of interest (ROI), and partial least squares discriminant analysis (PLS-DA) and back propagation neural networks (BPNN) discriminative models were established based on the full wavelength spectral information. By comparison, the optimal discriminant model was obtained; (2) Characteristic wavelength was extracted by competitive adaptive reweighting sampling (CARS), and BPNN discriminant model was established; (3) The data compression of the single band images was carried out by principal component analysis, and the *Cerasus Humilis* fruit defects was discriminated using the principal component image of both BPNN and a CNN; (4) By comparing the classification results of different methods, select the best model for identifying defects in *Cerasus Humilis* fruit.

MATERIALS AND METHODS

Experimental Sample

The "Nongda No. 6" *Cerasus Humilis* fruit samples were collected from the *Cerasus Humilis* planting base in the agricultural high-tech industry demonstration zone of Jinzhong, China. To ensure the consistency of the samples and reduce the impact of sample differences on the study, the principles of picking were similar shapes, uniform size (9.0-13.0g per fruit), and complete defect types (intact, rust spots, insect damage, cracks) are followed.

On the day of harvest, the samples were transported to the laboratory and screened. A total of 420 samples were selected and divided into intact and defective groups. Among them, 160 were intact *Cerasus Humilis* fruits, while the defective group included 92 rust spot fruits, 84 insect damage fruits, and 84 crack fruits. The intact and three types of defective samples were shown in Fig. 1.

a) Intact sample *b) Rust spot sample* *c) Insect damage sample* *d) Crack sample*

Fig. 1 - Figure of intact and defective samples of *Cerasus Humilis* fruit

Rust spots are the spots formed on the surface of fruits after being damaged by pests and diseases. Cracked fruit is a type of fruit that encounters rainy weather during its ripening period. With the rapid expansion of the flesh, the skin of the fruit will crack in different sizes and shapes, exposing the flesh tissue and causing the fruit to begin to decay. Insect damage fruit refers to its larvae often drilling holes on the surface of the fruit to feed inside, resulting in low fruit yield and loss of commercial value.

Reasonable and effective sample set partitioning is of great significance for the model establishment and can improve model discrimination accuracy. Collect hyperspectral images of each sample and assign values of 1, 2, 3, and 4 to four types of data (rust spot fruit, cracked fruit, insect damage fruit, and intact fruit).

Using the SPXY algorithm, each type of sample was randomly divided into a correction set and a prediction set according to the ratio of 3:1 *(Galvao et al., 2005)*, with 315 samples as the correction set and 105 samples as the prediction set. The statistical results of sample set partitioning were shown in Table 1.

Table 1

The sample set results were divided by the SPXY algorithm

Type	No. of samples	Correction set	Prediction set
Rust spot	92	69	23
Crack	84	63	21
Insect damage	84	63	21
Intact	160	120	40
Total	420	315	105

Instruments and Equipment

The "Gaia" hyperspectral imaging system developed by Beijing Zhuoli Hanguang Company was used in this study, with a wavelength range of 900~1700 nm, and the schematic of the system was shown in Fig. 2. It mainly consists of an Image-k-N17E spectral camera, four 35 W bromide tungsten lamps, a computer, an electric mobile platform, and a dark box. To avoid information oversaturation and imaging distortion, after multiple experiments, it was finally determined that the exposure time t=150 ms, the distance between the sample and the lens h=280 mm, and the conveyor belt movement speed v=8.0 mm/s. When obtaining hyperspectral images, a self-made perforated carrier plate was placed on the platform, and the tested sample was placed horizontally on the carrier platform. For the tested samples with defects, the defect area was manually oriented and the target area was oriented towards the camera. The images of the samples obtained in the hyperspectral imaging system was shown in Fig. 3.

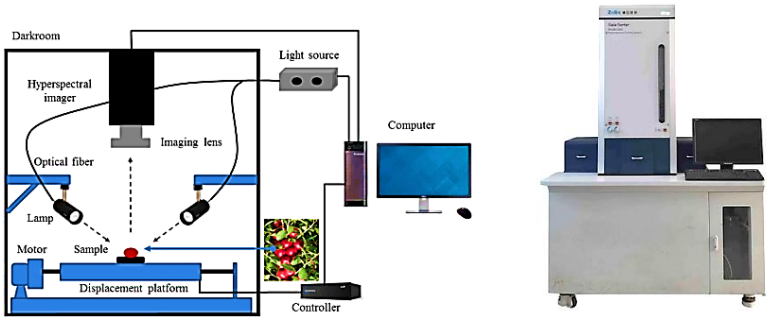

Fig. 2 - Experiment platform of the hyperspectral imaging system

a) Intact sample *b) Rust spot sample* *c) Insect damage sample* *d) Crack sample*

Fig. 3 - Hyperspectral Images of *Cerasus Humilis* fruit Samples

Correction Method of Hyperspectral Image

In order to eliminate the influence of changes in light intensity and dark currents in the lens on imaging, as well as to calculate the relative reflection spectrum value of the scanned object, it is necessary to perform black and white board correction before the spectral acquisition *(Baranowski et al., 2012)*. The calculation formula is shown in Equation (1):

$$I_C = \frac{I_R - I_D}{I_W - I_D} \times 100\% \quad (1)$$

where I_C represents the corrected image, I_R represents the original image, I_D represents the black reference image, and I_W represents the white reference image.

Statistical Analysis

This study used the CARS algorithm to extract characteristic wavelengths and modeled them using PLSDA, BPNN, and CNN. CARS is a new variable optimization method *(Ma et al., 2019)*, which imitates the principle of "survival of the fittest" in Darwin's evolution theory. Using adaptive reweighted sampling (ARS) technology, each wavelength was treated as a separate individual, and variables with large absolute values of regression coefficients are selected from the PLS model. Variables with small absolute values of regression coefficients are eliminated, and a series of wavelength variable subsets were obtained through multiple repeated screenings. The subset of variables with the smallest root mean square error in the PLS model was selected through cross-validation with ten folds, which was the optimal wavelength variable quantum set *(Wieme et al., 2022).*

PLS-DA is a multivariable statistical analysis method combining the partial least squares method and linear discriminant analysis method *(Yan et al., 2020)*. It uses cross-validation to obtain the optimal number of principal components, and then carries out linear discriminant analysis to solve the problem of independent variable multicollinearity in regression analysis. In this study, principal components were selected based on interaction testing, with a maximum principal component score of 10, and a 10-fold interaction test was performed.

BPNN is a multi-layer feedforward neural network trained according to the error backpropagation algorithm *(Li et al., 2017)*. It can arbitrarily complex pattern classification and excellent multidimensional function mapping and solves the XOR and other problems that cannot be solved by simple perceptron. In this study, the activation function of the hidden layer and output layer of the network was set as tansing and purelin functions, respectively. The network training function was trainlm function, and the number of neurons in the hidden layer was set as 6. The number of network iterations was 2500, an expected error of 0.001, and a learning rate of 0.1.

The basic structure of CNN includes a feature extraction layer and a feature mapping layer, which is an improvement based on BP neural network *(Xu et al., 2020)*. In CNN, the perception area of a neural unit comes from the part of the upper neural units. The same feature plane realizes weight sharing, which reduces the complexity of the network and the risk of overfitting. In this study, the structure of CNN includes an input layer, a 2-layer convolution layer, a down-sampling layer, a full connection layer, and an output layer. See Fig. 4 for the basic structure.

The input image size is 36×36, the feature mapping structure uses the sigmoid function with a small influence function kernel as the activation function of the convolution network. The number of feature maps of the first convolution is 4, the number of feature maps of the second convolution is 8, the size of the convolution kernel is 5×5, the size of the convolution kernel for down-sampling layer was 2×2, with a learning efficiency of 0.1. The number of training samples in each batch was 10, and the number of iterations in each batch was 720.

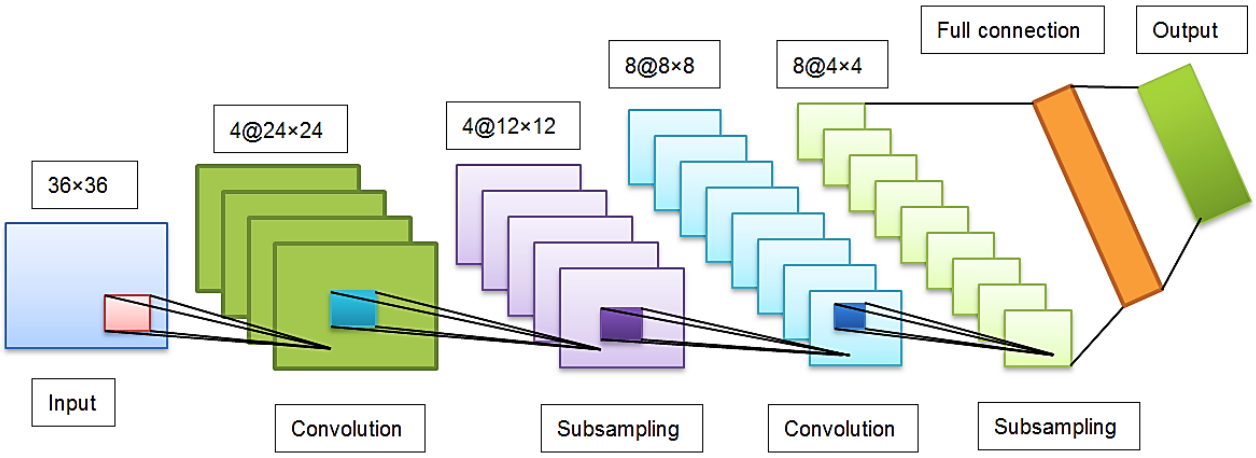

Fig. 4 - CNN structure

EXPERIMENTAL RESULTS AND ANALYSIS

Spectral Characteristics and Analysis

Using ENVI software to extract spectral information of the region of interest of the samples, the original spectral curves of 420 samples were shown in Fig. 5(a). Then calculate the average spectra of each sample as spectral information, as shown in Fig. 5 (b). Remove the bands containing a large amount of noise and only retain the wavelength range of 945-1675 nm (230 bands) for subsequent research.

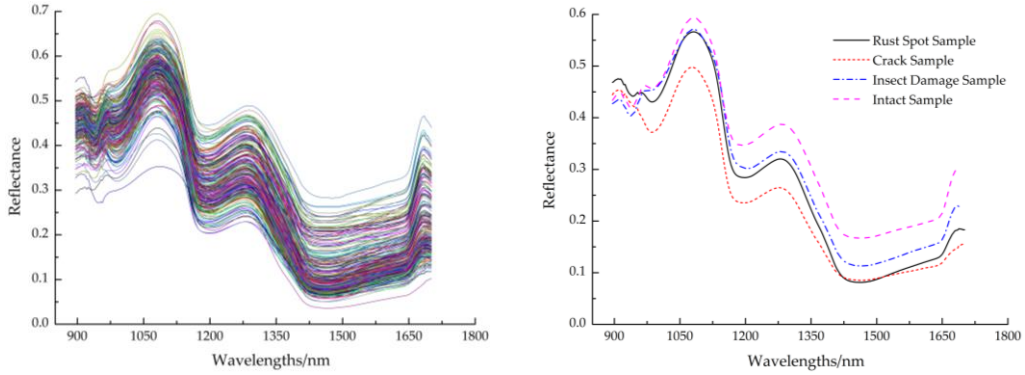

a) Original spectral curve *b) Average raw spectra curve*

Fig. 5 - Spectral curves of four different *Cerasus Humilis* fruit samples

From the spectrogram Fig. 5, it can be seen that the spectra of all four types of samples exhibit similar spectral features and curve shapes. From Fig. 5(a), it can be seen that the absorption peaks at 980 nm and 1195 nm are related to the second overtone of O-H stretching and the second overtone of C-H stretching, respectively *(Liu et al., 2010)*. There is a clear absorption peak at about 1460 nm, which was related to the first overtone of bond O-H *(Osborne et al., 2006)*. From Fig. 5(b), it can be seen that the spectral reflectance values of all defective samples are significantly lower than those of intact samples. This may be because the gray value of defective regions is usually lower, reducing the reflection of incident light *(Li et al., 2012)*.

Discriminative Model Based on Full Wavelengths Spectral Information

Linear (PLS-DA) and nonlinear (BPNN) discriminative models were established based on the full wavelength spectral information. When the discriminative model was established to discriminate the type of samples if the correct prediction value of the rust blotch is within the threshold value [0.5, 1.5], it is determined that the prediction category is consistent with the assumed category, that is, it is determined as the rust spotted fruit. By analogy, the threshold range for cracked fruit was (1.5, 2.5], the threshold range for insect-infested fruit was (2.5, 3.5], and the threshold range for intact fruits was (3.5, 4.5]. Compare and analyze the discriminant classification performance of the established models.

PLS-DA Discriminative Model

With the full wavelength spectral data as the input of the PLS-DA model, a PLS-DA prediction discriminative model was established to discriminate the prediction set of *Cerasus Humilis* fruit samples. During the modeling process, 10 times of cross-validation was selected to prevent overfitting, and the latent variables (Lvs) value was within the range of 2~20. When Lvs was 12, the PLS-DA model had the highest discrimination accuracy, as shown in Table 2.

Table 2

Discrimination results for defect types of *Cerasus Humilis* fruits by PLS-DA model

Type	Number of predicted samples	Misjudgment samples	Accuracy (%)
Rust spot	23	6	73.91
Crack	21	5	76.19
Insect damage	21	5	76.19
Intact	40	1	97.50

Total	105	17	83.81

From Table 2, it can be seen that the PLS-DA model had a good discrimination effect on the prediction set. The discrimination accuracy of this model for rust spot fruit, cracked fruit, insect damage fruit, and intact fruit was 73.91%, 76.19%, 76.19%, and 97.50%, respectively, with an overall accuracy of 83.81%. The total number of misjudged samples in the prediction set by this model was 17. Among them, 6 rust spot fruit were misjudged as intact due to their small rust area, 5 cracked fruits were misjudged as insect damage fruit due to their small cracks, 5 insect damage fruit were misjudged as intact due to their small insect damage area, and 1 intact fruit was not detected.

BPNN Discriminative Model

A BPNN discriminative model for the defect types of *Cerasus Humilis* fruits was established by using Matlab software. The number of input nodes of the model was determined by the data dimension of the full spectrum input, and the number of output nodes was determined by the defect types of *Cerasus Humilis* fruits, that is, the number of model output nodes was 4. Normalize the input data matrix to distribute the data within the range of [-1, 1]. The discrimination results of this model for four types of *Cerasus Humilis* fruit defect samples were shown in Table 3.

Table 3

Discrimination results for defect types of *Cerasus Humilis* fruits by BPNN model

Type	Predicted samples	Misjudgment	Accuracy (%)
Rust spot	23	6	73.91
Crack	21	4	80.95
Insect damage	21	4	80.95
Intact	40	1	97.50
Total	105	15	85.71

From Table 3, it can be seen that the BPNN model had a good discrimination effect on the prediction set, but the model required a longer training time. The discrimination accuracy of this model for rust spot fruit, cracked fruit, insect damage fruit, and intact fruit was 73.91%, 80.95%, 80.95%, and 97.50%, respectively, with an overall correct discrimination rate of 85.71%. The total number of misjudged samples in the prediction set by this model was 15. Among them, 6 rust spot fruit were misjudged as intact due to their small rusty area, 4 cracked fruits were misjudged as insect damage fruit due to their small cracks, 4 insect damage fruit was misjudged as intact due to their small insect damaged area, and 1 intact fruit was not detected.

Characteristic Wavelength Extraction

The purpose of feature extraction is to extract effective information from the original standard sample spectrums, overcome the linear correlation, singularity, and instability of the original spectrum data, and improve prediction reliability. When extracting feature spectra, it is necessary to minimize the dimensionality of the data or the number of variables, while also minimizing the omission of useful explanatory information.

The results of the CARS algorithm (with Monte Carlo sampling number N=50) running in Matlab R2014b software were shown in Fig. 6, where Fig. 6(a) reflected a continuous decrease in the number of wavelength variables filtered as the sampling number increases, and the rate of decrease from fast to slow. In Fig. 6(b), it can be seen that during the 1~43 sampling process, RMSECV showed a downward trend, reflecting that the eliminated variables in this process were information unrelated to the identification of defect features of *Cerasus Humilis* fruits. Starting from the 44th sampling, RMSECV gradually increased, reflecting that this screening process began to eliminate useful information related to the identification of defect features of *Cerasus Humilis* fruits. Fig. 6(c) showed the trend of the regression coefficients of each wavelength variable during the process of wavelength variable optimization. The vertical line position marked with "*" in the figure indicated that when the number of sampling runs was 43, the RMSECV reached the minimum value of 0.4298.

At this time, the eight characteristic wavelengths selected by CARS were 950, 994, 1071, 1263, 1336, 1457, 1542, and 1628 nm, respectively.

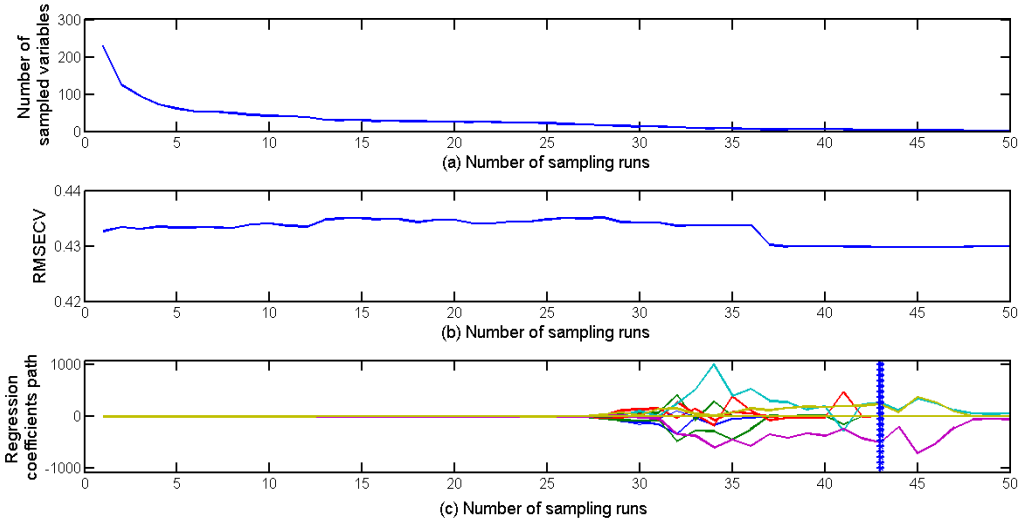

Fig. 6 - Process of selecting characteristic wavelength by CARS method

Based on the characteristic wavelength extracted by the CARS algorithm, a BPNN discriminative model was established. When the mean square error was 0.0028 and the number of iterations was 12, the discrimination accuracy of the CARS-BPNN model was 90.47%. This indicated that the characteristic wavelength had a better modeling effect than the full wavelength, and there was some noise in the full wavelength of this study. Therefore, the selection of effective variable information, the improvement of computational speed, and the stability and reliability of algorithms were also important influencing factors for model stability.

The CNN Recognition Model Based on Image Information

Principal component analysis (PCA) is a widely used method for data dimensionality reduction and feature extraction, which helps to enhance target area information and remove noise. PCA converts raw data into linearly independent variables, known as principal components (PCs). Perform principal component analysis on the images corresponding to the 8 characteristic wavelengths extracted by CARS and obtain the cumulative principal component contribution values of intact and defective *Cerasus Humilis* fruit samples, as shown in Table 4. From Table 4, it can be concluded that the cumulative contribution rate of the first six PCs had reached 99.82%, which can effectively explain the sample information variables. Therefore, the first six principal components were selected for analysis.

Table 4

The cumulative contribution rate of the first eight principal components of the image

PCs	Characteristic Value	Contribution Rate (%)
1	28924.1723	81.78
2	8847.3621	93.62
3	1035.3651	95.35
4	753.5245	96.92
5	186.7485	98.62
6	70.7625	99.82
7	9.6372	99.99
8	1.8674	100.00

Fig. 7 showed the first eight PC images based on intact and defective *Cerasus Humilis* fruits in the feature band. Different PC images reflect different *Cerasus Humilis* fruit defect features. These PC images

were sorted according to the degree of decreasing variance, with the first PC image having the highest proportion of variance and containing the most original information.

From Fig. 7, it can be seen that the top 6 PC images (PC-1 to PC-6) of four different defect types of *Cerasus Humilis* fruit had the most original image information, while PC-7 to PC-8 images contain more noise and no longer have meaningful information for detecting surface defect features of *Cerasus Humilis* fruit. Through rapid visual inspection of the top 6 PC images, it was found that in some converted partial PC images, the main defect features became more prominent, indicating that PCA can extract useful features. Therefore, PC-3 images of cracked fruits, PC-5 images of insect-infested fruits, PC-6 images of rusty fruits, and PC-6 images of intact fruits were selected for analysis. Simultaneously extract the grayscale values of each sample PC image and normalize the data, and establish a classification model using BPNN and CNN.

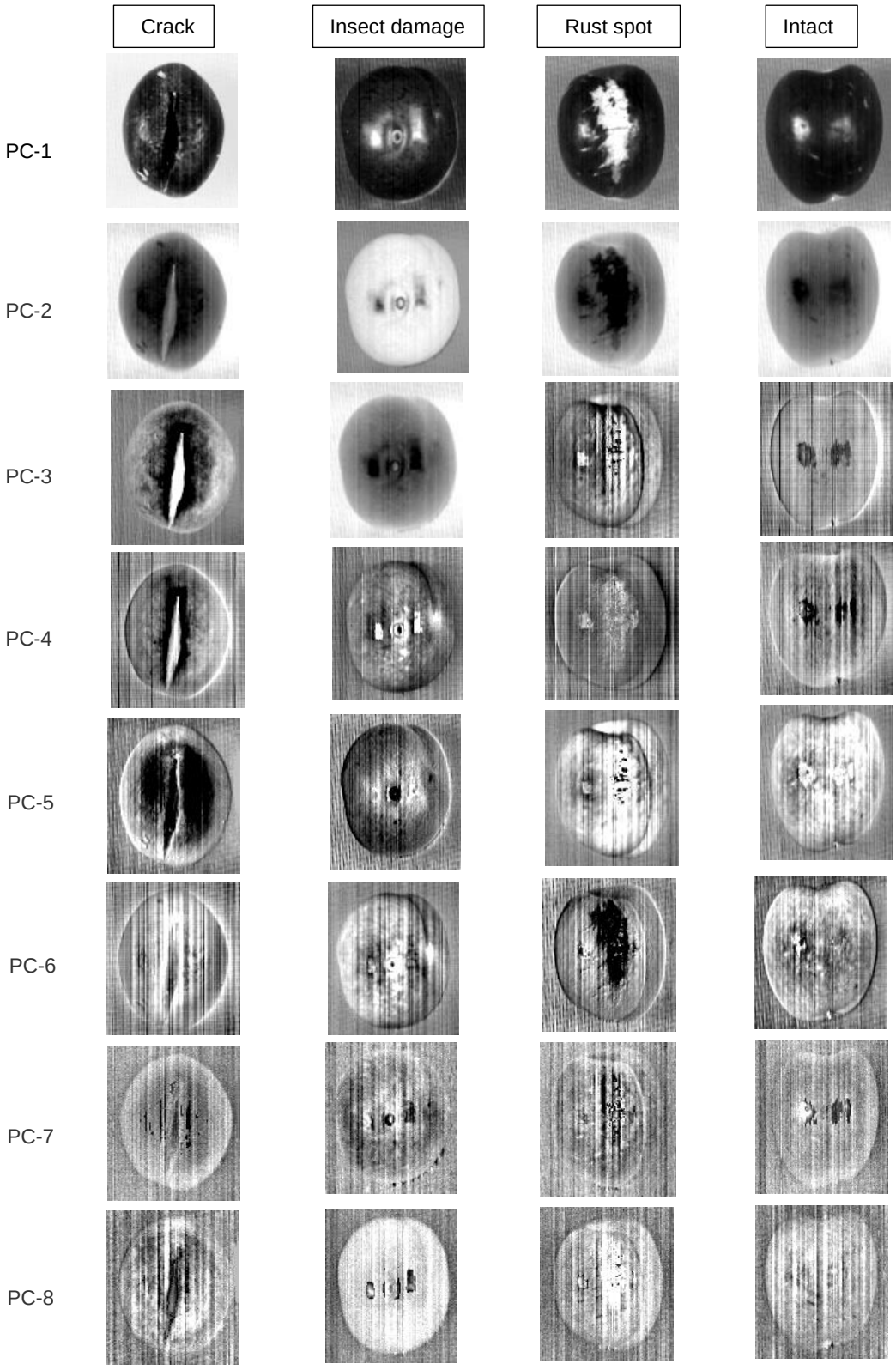

Fig. 7 - The first eight PCs grayscale images of *Cerasus Humilis* fruit based on the special bands

The discrimination results of the BPNN and CNN models established based on principal component images were shown in Table 5. When the root mean square error of the BPNN model was 0.97 and the number of iterations was 5, the discrimination accuracy reached 83.81%. Four intact fruits were misclassified as rust spot fruits, five rust spot fruits were identified as intact fruits, four insect damage fruits were misclassified as intact fruits, and four cracked fruits were not detected. In CNN discriminative model, with the increase of learning times, the mean square error showed a downward trend on the whole and converges to a stable value when the number of iterations was 14226.

When the number of iterations is 23610 and the mean square error is 0.0063, the discrimination accuracy was 93.33%. Two intact fruits were misclassified as rust spot fruits, three rust spot fruits were misclassified as intact fruits, one insect damage fruit was misclassified as intact fruit, and one cracked fruit was not detected. The discrimination accuracy of the CNN model was significantly better than that of BPNN, and it had good application prospects in agricultural product quality detection based on hyperspectral imaging technology. The CARS-BPNN defect recognition based on spectral information and the CNN recognition based on image information has achieved good results.

Based on this, future research will establish a stable model suitable for online sorting in industrial production.

Table 5

The results of BPNN and CNN models

Models	Epochs	Mean square error	Accuracy (%)
BPNN	5	0.97	83.81
CNN	23610	0.0063	93.33

DISCUSSION

In this study, hyperspectral technology combined with convolutional neural network was used to identify the defective *Cerasus Humilis* fruit. Different detection models were established from two angles of spectral information and image information, and the optimal detection model was determined by comparison. Both CARS-BPNN based on spectral information and CNN based on image information has achieved good results in identifying defective *Cerasus Humilis* fruit. When the number of iterations is 23610 and the mean square error is 0.0063, the discrimination accuracy of the CNN model was 93.33%. *Sun et al. (2018)* detected black spot disease in fresh jujube based on hyperspectral and convolutional neural networks, and collected the information of intact and black spot fresh jujube in different years.

The results show that the discrimination accuracy of the CNN model based on principal component images was 90.0%. *Liu et al. (2018)* collected hyperspectral image information of 5 types of cucumbers (normal, watery, split/hollow, shrivel, and surface defect) and developed a classification algorithm that the SSAE combined with convolutional neural network (CNN-SSAE) learning.

The results showed that the overall classification accuracy of CNN- SSAE for defective cucumbers was 91.1%. *Chen et al. (2023)* combined hyperspectral imaging technology with convolutional neural network to conduct real-time detection of egg defects and freshness. The research results indicate that the overall accuracy of one-dimensional convolutional neural networks (1D-CNN) for egg freshness and defect detection were 99% and 100%, respectively. *Pham et al. (2022)* proposed to combine convolutional neural networks with hyperspectral image information to classify the surface defect types of red jujube. The results show that, compared with the traditional machine learning method, the detection accuracy of CNN was 94.5%, and the classification time was reduced to 16.6 s. Compared with the above research results, this study also achieved good results in the identification of *Cerasus Humilis* fruit defects, but there are still missing detection phenomena.

Finally, the research shows that CNN could better detect the defect types of fruits and vegetables. However, compared with relevant researchers *(Chen et al., 2023)*, the detection accuracy of the results was slightly lower of this study (93.33%). This may be due to the small size and the irregular defect area on the fruit surface of this study object, resulting in a slightly lower recognition rate. The subsequent research will improve the image recognition algorithm to improve the recognition rate.

CONCLUSIONS

This study was based on hyperspectral imaging technology for identifying defective *Cerasus Humilis* fruit. PLS-DA and BPNN were used to establish a full band recognition model, and the discrimination accuracy of PLS-DA and BPNN models was above 83.00%. CARS were used to extract feature wavelengths and a CARS-BPNN model was established, with a recognition accuracy of 90.47%, which was significantly better than the models built for all bands. Based on the feature wavelengths extracted by CARS, principal component images were obtained, and recognition models were established using BPNN and CNN, with discrimination

accuracy rates of 83.81% and 93.33%, respectively. Both CARS-BPNN based on spectral information and CNN based on image information have achieved good results in identifying defective *Cerasus Humilis* fruit. Therefore, the combination of hyperspectral imaging technology and CNN had good application prospects in the classification of agricultural products, providing a theoretical basis for further designing classification devices and achieving real-time online sorting in industrial production.

However, the *Cerasus Humilis* fruits of similar weight and size were selected as research objects in this study, and the influence of different sizes and varieties, growing environment, and more defect types of *Cerasus Humilis* fruit on the identification accuracy was not considered. In the later stage, hyperspectral image information of various types of *Cerasus Humilis* fruit will be collected considering the influence of the above factors, and combined with deep learning algorithm, the optimal model will be found by adjusting model parameters, and its defects and varieties will be identified.

ACKNOWLEDGEMENT

This work was funded by Basic Research Project of Shanxi Province (Free Exploration) (Project No. 202203021212426), "Introduction of Talents and Scientific Research Initiation Project" of Shanxi Agricultural University (Project No. 2023BQ42).

REFERENCES

[1] Baranowski, P., Mazurek, W., Wozniak, J., & Majewska, U. (2012). Detection of early bruises in apples using hyperspectral data and thermal imaging. *Journal of Food Engineering*, *110*(3), 345-355. https://doi.org/10.1016/j.jfoodeng.2011.12.038

[2] Chen, C., Jiang, F., Yang, C., Rho, S., Shen, W., Liu, S., & Liu, Z. (2018). Hyperspectral classification based on spectral–spatial convolutional neural networks. *Engineering Applications of Artificial Intelligence*, *68*, 165-171. https://doi.org/10.1016/j.engappai.2017.10.015

[3] Chen, S. Y., Hsu, S. H., Ko, C. Y., & Hsu, K. H. (2023). Real-time defect and freshness inspection on chicken eggs using hyperspectral imaging. *Food Control*, *150*, 109716. https://doi.org/10.1016/j.foodcont.2023.109716

[4] Fazari, A., Pellicer-Valero, O. J., Gómez-Sanchıs, J., Bernardi, B., Cubero, S., Benalia, S., ... & Blasco, J. (2021). Application of deep convolutional neural networks for the detection of anthracnose in olives using VIS/NIR hyperspectral images. *Computers and Electronics in Agriculture*, *187*, 106252. https://doi.org/10.1016/j.compag.2021.106252

[5] Fu, L., Feng, Y., Liu, Z., Li, R., & Cui, Y. (2018). Image recognition method of multi-cluster kiwifruit in field based on convolutional neural networks. *Transactions of the Chinese Society of Agricultural Engineering*, *34*(2), 205-211. https://doi.org/10.11975/j.issn.1002-6819.2018.02.028

[6] Gai, Z., Sun, L., Bai, H., Li, X., Wang, J., & Bai, S. (2022). Convolutional neural network for apple bruise detection based on hyperspectral. *Spectrochimica Acta Part A: Molecular and Biomolecular Spectroscopy*, *279*, 121432. https://doi.org/10.1016/j.saa.2022.121432

[7] Galvao, R. K. H., Araujo, M. C. U., José, G. E., Pontes, M. J. C., Silva, E. C., & Saldanha, T. C. B. (2005). A method for calibration and validation subset partitioning. *Talanta*, *67*(4), 736-740. https://doi.org/10.1016/j.talanta.2005.03.025

[8] Gao, Q., Wang, P., Niu, T., He, D., & Zhao, X. (2022). Soluble solid content and firmness index assessment and maturity discrimination of Malus micromalus Makino based on near-infrared hyperspectral imaging. *Food Chemistry*, *370*, 131013. https://doi.org/10.1016/j.foodchem.2021.131013

[9] Jiang, M., Li, Y., Song, J., Wang, Z., Zhang, L., Song, L., & Pan, L. (2023). Study on Black Spot Disease Detection and Pathogenic Process Visualization on Winter Jujubes Using Hyperspectral Imaging System. *Foods*, *12*(3), 435. https://doi.org/10.3390/foods12030435

[10] Khaw, H.Y., Soon, F.C., Chuah, J.H., & Chow, C.O. (2017). Image noise types recognition using convolutional neural network with principal components analysis. *IET Image Processing*, *11*(12), 1238-1245. https://doi.org/10.1049/iet-ipr.2017.0374

[11] Li, J., Rao, X., & Ying, Y. (2012). Development of algorithms for detecting citrus canker based on hyperspectral reflectance imaging. *Journal of the Science of Food and Agriculture*, *92*(1), 125-134. https://doi.org/10.1002/jsfa.4550

[12] Li, Y., Lu, W., Zhao, J., Feng, G., Wei, D., Lu, J., & Lu, Z. (2017). Detection of caloric value of coal using laser-induced breakdown spectroscopy combined with bp neural networks. *Spectroscopy and Spectral Analysis*, *37*(08), 2575-2579. https://doi.org/10.3964/j.issn.1000-0593(2017)08-2575-05

[13] Liu, G., He, J., Wang, S., Luo, Y., Wang, W., Wu, L., & He, X. (2016). Application of near-infrared hyperspectral imaging for detection of external insect infestations on jujube fruit. *International Journal of Food Properties*, *19*(1), 41-52. https://doi.org/10.1080/10942912.2014.923439

[14] Liu, Y., Sun, X., Zhang, H., & Aiguo, O. (2010). Nondestructive measurement of internal quality of Nanfeng mandarin fruit by charge coupled device near infrared spectroscopy. *Computers and Electronics in Agriculture*, *71*, S10-S14. https://doi.org/10.1016/j.compag.2009.09.005

[15] Liu, Z., He, Y., Cen, H., & Lu, R. (2018). Deep feature representation with stacked sparse auto-encoder and convolutional neural network for hyperspectral imaging-based detection of cucumber defects. *Transactions of the ASABE*, *61*(2), 425-436. https://doi.org/10.13031/trans.12214

[16] Ma, W., Zhang, M., Li, Y., Yang, L., Zhu, Z., & Cui, K. (2019). Non-destructive Detection for Fat Content of Walnut Kernels by Near Infrared Spectroscopy. *Transactions of the Chinese Society for Agricultur*al Machinery, 50(3), 374-379. https://doi.org/10.6041/j.issn.1000-1298.2019.S0.057

[17] Osborne, B. G. (2006). Near-infrared spectroscopy in food analysis. Encyclopedia of analytical chemistry: applications, theory and instrumentation. https://doi.org/10.1002/9780470027318.a1018

[18] Pham, Q. T., & Liou, N. S. (2022). The development of on-line surface defect detection system for jujubes based on hyperspectral images. *Computers and Electronics in Agriculture*, *194*, 106743. https://doi.org/10.1016/j.compag.2022.106743

[19] Singh, T., Garg, N. M., & Iyengar, S. R. (2021). Nondestructive identification of barley seeds variety using near-infrared hyperspectral imaging coupled with convolutional neural network. *Journal of Food Process Engineering*, *44*(10), e13821. https://doi.org/10.1111/jfpe.13821

[20] Sun, H., Zhang, S., Liu, J., Chen, C., & Xing, S. (2018). Detection of black rot of fresh jujube fruits using hyperspectral imaging and a convolutional neural network. *Journal of Shanxi Agricultural University*, *38*(11), 15-19. https://doi.org/10.13842/j.cnki.issnl671-8151.201807021

[21] Wang, B., Yang, H., & Li, L. (2023). Discrimination of cerasus humilis fruit maturity based on hyperspectral imaging technology. *INMATEH-Agricultural Engineering*, *70*(2), 107-116. https://doi.org/10.35633/inmateh-70-10

[22] Wang, B., Yang, H., Zhang, S., & Li, L. (2023). Detection of Defective Features in Cerasus Humilis Fruit Based on Hyperspectral Imaging Technology. *Applied Sciences, 13*(5), 3279. https://doi.org/10.3390/app13053279

[23] Wieme, J., Mollazade, K., Malounas, I., Zude-Sasse, M., Zhao, M., Gowen, A., ... & Van Beek, J. (2022). Application of hyperspectral imaging systems and artificial intelligence for quality assessment of fruit, vegetables and mushrooms: A review. *Biosystems Engineerin*g, *222*, 156-176. https://doi.org/10.1016/j.biosystemseng.2022.07.013

[24] Xu, J., Shao, M., Wang, Y., & Han, W. (2020). Recognition of corn leaf spot and rust based on transfer learning with convolutional neural network. *Transactions of the Chinese Society for Agricultural Machinery*, *51*(2), 230-236+253. https://doi.org/10.6041/j.issn.1000-1298.2020.02.025

[25] Xue, Y., Wang, L., Zhang, Y., & Shen, Q. (2020). Defect detection method of apples based on GoogLeNet deep transfer learning. *Transactions of the Chinese Society for Agricultural Machinery*, *51*(7), 30-35. 10.6041/j.issn.1000-1298.2020.07.004

[26] Yan, L., Pang, L., Wang, H., & Xiao, J. (2020). Recognition of different Longjing fresh tea varieties using hyperspectral imaging technology and chemometrics. *Journal of Food Process Engineering*, *43*(4), e13378. https://doi.org/10.1111/jfpe.13378

[27] Ye, S., & Weng, H. (2022). Identification of Grapefruit Black Spot Based on Hyperspectral Imaging using Naïve-Bayes Classifier. Agricultural Mechanization, *Electrification and Automation*, *1*(1), 1-9. https://doi.org/10.23977/hyde.2022.010101

[28] Yu, K., Zhao, Y., Li, X., Shao, Y., Zhu, F., & He, Y. (2014). Identification of crack features in fresh jujube using Vis/NIR hyperspectral imaging combined with image processing. *Computers and Electronics in Agriculture*, *103*, 1-10. https://doi.org/10.1016/j.compag.2014.01.016

[29] Zhang, Y., Wang, W., Zhang, F., Ma, Q., Gao, S., Wang, J., & Liu, Y. (2022). Rapid and non-destructive decay detection of Yali pears using hyperspectral imaging coupled with 2D correlation spectroscopy. *International Journal of Agricultural and Biological Engineering*, *15*(5), 236-244. https://doi.org/10.25165/j.ijabe.20221505.7313

[30] Zhu, S., Zhou, L., Zhang, C., Bao, Y., Wu, B., Chu, H., & Feng, L. (2019). Identification of soybean varieties using hyperspectral imaging coupled with convolutional neural network. *Sensors*, *19*(19), 4065. https://doi.org/10.3390/s19194065